

Review

# Mechanical Properties of Aramid Fiber Fabrics and Composites Enhanced by Phthalic Anhydride Catalyzed with Anhydrous Aluminum Chloride

Yi Xiao <sup>1</sup>, Yibo E <sup>1</sup>, Hanmei Gao <sup>1</sup>, Honggang Li <sup>1</sup>, Guowen Xu <sup>2</sup> and Xuhong Qiang <sup>3,\*</sup><sup>1</sup> Research Center for Composite Materials, Science and Engineering of Composite Materials, Shanghai University, Shanghai 201900, China; [yixiao@shu.edu.cn](mailto:yixiao@shu.edu.cn) (Y.X.)<sup>2</sup> Engineering Research Institute of China Construction Eighth Engineering Division, Shanghai 200122, China<sup>3</sup> College of Civil Engineering, Tongji University, Shanghai 200092, China\* Correspondence: [qiangxuhong@tongji.edu.cn](mailto:qiangxuhong@tongji.edu.cn)

**Abstract:** The surface modification of aramid fiber plain fabric (PPTA) was conducted through phthalic anhydride treatment and anhydrous aluminum chloride ( $\text{AlCl}_3$ ) catalysis, aiming to enhance the interfacial bonding strength between aramid fiber fabric and bisphenol A diglycidyl ether (DGEBA) resin. The surface morphologies and structures of PPTA fiber before and after modification were characterized using scanning electron microscopy, atomic force microscopy, X-ray photoelectron spectroscopy, and X-ray diffractometry. The mechanical properties of the PPTA/DGEBA composite were evaluated using a universal mechanical testing machine. The results demonstrate that when the concentration of phthalic anhydride is 0.3 mol/L, the tensile strength, bending strength and interlaminar shear strength of PPTA/DGEBA composites reach the maximum value, which are increased by 17.94%, 44.18%, and 15.94% compared with the unmodified sample, respectively. After a 0.5-h catalytic modification, the PPTA/DGEBA composites exhibited significantly enhanced tensile strength, bending strength, and interlaminar shear strength, achieving respective increments of 32.28%, 24.91%, and 29.10% compared to the modified samples without catalyst addition. Moreover, the overall mechanical properties of the aramid fiber fabrics and composites were substantially improved, which are more suitable for structural applications.



**Citation:** Xiao, Y.; E, Y.; Gao, H.; Li, H.; Xu, G.; Qiang, X. Mechanical Properties of Aramid Fiber Fabrics and Composites Enhanced by Phthalic Anhydride Catalyzed with Anhydrous Aluminum Chloride. *Appl. Sci.* **2024**, *14*, 3800. <https://doi.org/10.3390/app14093800>

Academic Editor: Asterios Bakolas

Received: 15 April 2024

Revised: 26 April 2024

Accepted: 28 April 2024

Published: 29 April 2024



**Copyright:** © 2024 by the authors. Licensee MDPI, Basel, Switzerland. This article is an open access article distributed under the terms and conditions of the Creative Commons Attribution (CC BY) license (<https://creativecommons.org/licenses/by/4.0/>).

## 1. Introduction

Aromatic polyamide fiber, abbreviated as aramid fiber (PPTA), is the second-generation high-performance reinforcement fiber following carbon fiber [1–3]. As one of the three major high-performance fibers in the world, aramid fiber possesses superior properties, such as low density, high tensile strength, high modulus, excellent thermal stability, abrasion resistance, chemical corrosion resistance, and outstanding ballistic performance [4–7]. Consequently, it is widely used in the manufacturing of advanced composite materials for aerospace, civil engineering, armored protection, and other fields [8–13]. However, in practical applications, due to the rigid molecular structure, high crystallinity, smooth surface, and low-molecular-surface active functional groups of aramid fiber, it exhibits certain drawbacks, such as surface chemical inertness [14,15]. This results in poor interfacial adhesion between the reinforcement phase and the resin matrix when used in composite materials, making it difficult to fully transfer stress and affecting the overall performance of the composite materials, thereby greatly limiting its further application [16–19]. Therefore, while fully exploiting the excellent mechanical properties of aramid fiber, improving the interfacial adhesion performance of fiber-reinforced resin-based composite materials has become a hot research topic both domestically and internationally [20–25]. Currently, the

most commonly used technique involves modifying the surface of aramid fiber through chemical or physical methods to enhance the interfacial adhesion performance of composite materials [26–30], such as acid treatment [31,32], acid anhydride etching [33], plasma modification [34,35], high-energy radiation modification [36], etc.

Different from the strong acid and acetic anhydride etching commonly used in many previous studies, the Friedel–Crafts acylation reaction refers to a type of reaction where hydrogen or other functional groups in aromatic compounds are replaced by acyl groups [37–39]. The reaction between phthalic anhydride and PPTA fiber is an example of the Friedel–Crafts acylation reaction. The amide bond ( $-\text{CO-NH}-$ ) in the molecular chain of PPTA fiber possesses strong electron-donating ability, which can induce changes in the electron cloud density of the benzene ring and enhance the reactivity of the ortho position of the benzene ring [40,41]. Under the action of electrophilic reagents (such as phthalic anhydride), acylation reactions occur, resulting in the generation of  $-\text{OH}$  groups [42,43]. At the same time, partial amide bonds undergo hydrolysis, leading to the formation of  $-\text{COOH}$  groups. The reaction mechanism is illustrated in Figure 1. The anhydrous  $\text{AlCl}_3$  is the most representative catalyst for acylation reactions, widely used to increase the yield of the reaction product (ortho-benzoylbenzoic acid) between benzene and phthalic anhydride [44]. However, there is currently no research on the use of anhydrous  $\text{AlCl}_3$  for the reaction between phthalic anhydride and PPTA fiber. The catalytic mechanism of anhydrous  $\text{AlCl}_3$  for acylation reactions involves the carbon of the acyl group ( $-\text{CONH}-$ ) on the benzene ring of PPTA fiber becoming a carbocation under the action of anhydrous  $\text{AlCl}_3$ , promoting the occurrence of aromatic electrophilic substitution reactions, effectively increasing the reaction rate and yield, thereby shortening the modification time, and introducing more polar oxygen-containing functional groups on the fiber surface, increasing the number of active sites on the fiber surface [45,46].

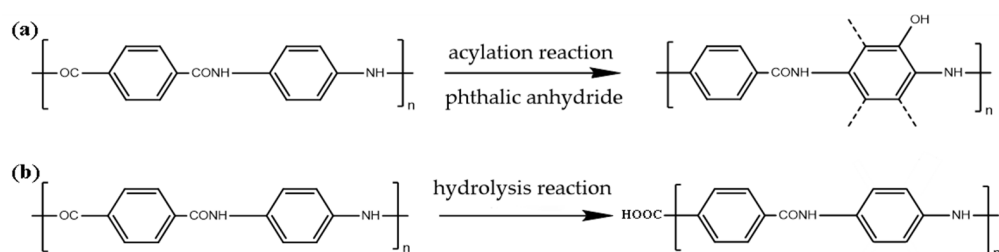


**Figure 1.** Reaction mechanism: (a) Acylation reaction; (b) Hydrolysis reaction.

This article investigates the effects of different concentrations of phthalic anhydride on etching plain-woven aramid fiber fabrics. Additionally, it innovatively explores the use of an anhydrous  $\text{AlCl}_3$ -catalyzed fiber modification process, examining the impact of different catalytic modification times on the performance of PPTA/DGEBA composite materials. Characterization is conducted using methods such as scanning electron microscopy (SEM), X-ray diffraction (XRD), X-ray photoelectron spectroscopy (XPS), atomic force microscopy (AFM), and universal mechanical testing machines. By altering the roughness of the fiber surface and increasing the contact area with the resin, the aim is to enhance the physical-mechanical interlocking and chemical bonding between the aramid fibers and DGEBA resin phases. This is intended to improve the interfacial bonding properties of the composite materials, thereby enhancing their overall performance.

## 2. Experimental Study

### 2.1. Materials and Reagents

The aramid fiber plain fabric (PPTA) was purchased from Yantai (Taihe New Material Co., Ltd., Yantai, China), and its performance parameters are presented in Table 1. Other chemical reagents used and purchasing units are as follows: bisphenol A diglycidyl ether (DGEBA), phthalic anhydride and anhydrous aluminum chloride were all sourced from Shanghai (Deborah Biotechnology Co., Ltd., Shanghai, China, McLin Biochemical

Technology Co., Ltd., Shanghai, China, Merrill Chemical Technology Co., Ltd., Sinopharm Chemical Reagent Co., Ltd., Shanghai, China). Anhydrous ethanol and acetone came from Sinopharm Chemical Reagent Co., Ltd., Shanghai, China. Among them, anhydrous ethanol was analytical grade (purity of 99.5%) and used as a solvent for phthalic anhydride, which is a surface modifier for aramid fiber plain fabric. Anhydrous aluminum chloride was used as a modification catalyst, and bisphenol A diglycidyl ether (EP) as the matrix of the aramid fiber composite material.

**Table 1.** PPTA fiber performance parameters.

Performance	Warp Direction	Latitudinal Direction
Single layer thickness (mm)	0.5	0.5
Mass per unit area ( $\text{g}/\text{m}^2$ )	340	340
Density (Yarns/10 cm)	150	148
Rupture strength (N/50 mm)	13,215	14,370
Elongation at break (%)	8.42	5.59
Coefficient of variation of fracture strength (%)	2.92	1.79

## 2.2. Experimental Method

### 2.2.1. PPTA Pretreatment

The PPTA fabric was immersed in a high-capacity beaker filled with acetone and placed inside an ultrasonic cleaner to eliminate any residual grease, ash layer, or other impurities that may have remained on the fiber surface during the spinning process. To prevent excessive volatilization of acetone caused by the heat generated from ultrasonic shock, the water in the ultrasonic container was replaced every 90 min to maintain a cooling effect. After undergoing 3 h of ultrasonic treatment, the fiber was removed and dried for 3 h at 100 °C in an air blast oven and cut into mold size for use.

### 2.2.2. Surface Modification of PPTA by Phthalic Anhydride

Under the influence of magnetic stirring, phthalic anhydride was dissolved in anhydrous ethanol to prepare solutions with mass concentrations of 0.15 mol/L, 0.3 mol/L, and 0.45 mol/L in each beaker, respectively. The pre-treated PPTA fabrics were immersed in each solution, respectively, with temperature modification at a constant 80 °C for 2 h (h). Afterward, the modified PPTA fabric was repeatedly cleaned with deionized water and placed in the oven at 100 °C for 3 h before use. In order to prevent the volatilization of the solution during the modification process, it was necessary to cover the beaker with a layer of plastic wrap.

### 2.2.3. Catalytic Modification of PPTA with Phthalic Anhydride by Anhydrous $\text{AlCl}_3$

Under the influence of magnetic stirring, phthalic anhydride was dissolved in anhydrous ethanol to prepare solutions with mass concentrations of 0.3 mol/L in a beaker. Then anhydrous  $\text{AlCl}_3$  was added to the phthalic anhydride solution. In order to prevent excessive reactivity, the addition of anhydrous  $\text{AlCl}_3$  to the phthalic anhydride solution was carried out gradually in batches. The total amount of anhydrous  $\text{AlCl}_3$  added was twice the mass of phthalic anhydride. The pre-treated PPTA fabrics were immersed in it and modified at 80 °C for 0.5 h, 1 h, 1.5 h, and 2 h, respectively. Similarly, the modified PPTA fabric was repeatedly cleaned with deionized water and placed in the oven at 100 °C for 3 h before use.

### 2.2.4. Preparation of PPTA-Reinforced Composite

In this experiment, unmodified and modified PPTA/DGEBA composite materials were all prepared by compression molding with a platen vulcanizing press. The ratio of DGEBA to the curing agent triethylene tetramine (TETA) was 10:1. The resin was applied to both sides of the fiber by a hand lay-up process. The composite materials used for the tensile, bending, and interlaminar shear tests consisted of 7 layers of PPTA fiber, with a

resin matrix content of approximately 20%. The molding process parameters are shown in Table 2.

**Table 2.** Molding process parameters.

Number of Fiber Layers	Molding Temperature ( $T_0$ ) °C	Molding Pressure ( $P_0$ ) MPa	Molding Time (t) h
7	60	5	2

### 2.3. Test Characterization Method

#### 2.3.1. Test Equipment

A 025MN flat vulcanizing machine (Wuxi Zhongkai Rubber Machinery Co., Ltd., Wuxi, China), Phenom Pro desktop scanning electron microscope (SEM, Phenom-World Shanghai Instruments Co., Ltd., Shanghai, China), attoDRY2100-9T atomic force microscope (AFM, Attocube Systems AG Co., Ltd., Haar, Germany), ESCALAB 250Xi X-ray photoelectron spectrometer (XPS, Thermo Fisher Scientific China, Ltd., Shanghai, China), D/MAX2500V+/PC X-ray diffractometer (XRD, Rigaku Corporation, Tokyo, Japan), and an MTS-CMT-4204 universal mechanical testing machine (Shenzhen Xin Sansi Experimental Instrument Co., Ltd., Shenzhen, China) were employed. Partial testing equipments are shown in Figure 2.

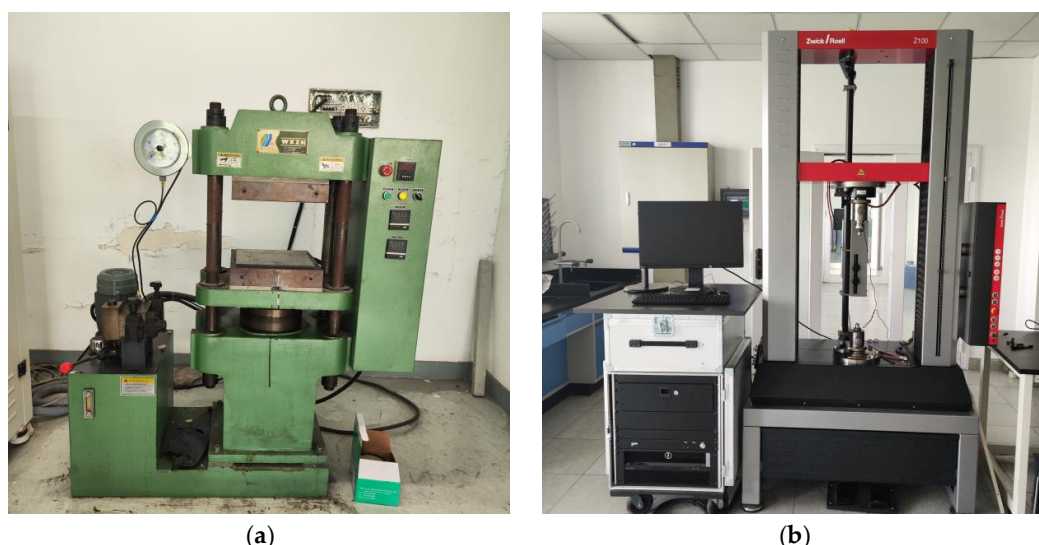


**Figure 2.** Partial testing equipment: (a) 025MN flat vulcanizing machine; (b) MTS-CMT-4204 universal mechanical testing machine.

#### 2.3.2. Characterization of Fiber Microstructure

A Phenom Pro desktop scanning electron microscope (SEM) and atomic force microscope (AFM) were employed to characterize the surface morphology and fracture morphology of aramid fiber before and after modification. The PPTA fibers were flatly fixed onto metal circular sample holders using conductive adhesive. After gold sputtering treatment, the surface microstructure of the PPTA fibers was observed using SEM. A scanning electron microscope/X-ray energy dispersive spectrometer (SEM/EDS) and an atomic force microscope (AFM) were employed to determine the surface element content and surface roughness of the fiber. For AFM analysis, the fibers needed to be trimmed to appropriate sizes and fixed onto the sample holder using double-sided adhesive. Care was taken to ensure that the entire surface of the sample remained at the same level. Tests were conducted using the tapping mode, with a scanning range of  $3 \times 3 \mu\text{m}$ .

X-ray diffraction (XRD) was used to analyze whether the modification treatment affected the crystal structure of aramid fibers, with a scanning speed of  $8^\circ/\text{min}$  and a scanning angle range from  $5^\circ$  to  $80^\circ$ .

X-ray photoelectron spectroscopy (XPS) was utilized to determine the surface elements, functional groups, and their content changes before and after modification of aramid fibers.

### 2.3.3. Mechanical Properties Tests of Composite Materials

A Shenzhen MTS-CMT-4204 electronic universal testing machine was used to test the tensile and bending properties of the PPTA/DGEBA composite materials. Testing was conducted according to the standards GB/T1040-2006 “*Determination of tensile properties of plastics*” and GB/T1449-2005 “*Test methods for flexural properties of fiber-reinforced plastics*”, respectively.

### 2.3.4. Interface Performance Tests of Composite Materials

Currently, the most widely used methods for interface evaluation in micro-composite material experiments are the single fiber pull-out test and the interlaminar shear strength (ILSS) test in macroscopic mechanical testing. The interlaminar shear strength (ILSS) of composite materials can reflect to a certain extent the interfacial bonding strength between the fibers and the resin matrix. In this experiment, an MTS-CMT-4204 electronic universal testing machine was utilized to test the interlaminar shear strength of PPTA/DGEBA composite materials, thereby characterizing the bonding performance of the composite material interfaces.

The interlaminar shear strength test was conducted in accordance with ASTM D2344 “*Standard Test Method for Short-Beam Strength of Polymer Matrix Composite Materials and Their Laminates*”. The specimen dimensions were 12 mm × 4 mm × 2 mm, with a span-to-depth ratio of 4:1, and the testing speed was set to 1 mm/min. The interlaminar shear strength value was calculated according to Equation (1).

$$F = 0.75 \times \frac{P_m}{b \times h} \quad (1)$$

where  $F$  is the interlaminar shear strength (MPa);  $P_m$  is the maximum load (N);  $b$  is the specimen width (mm), and  $h$  is the specimen thickness (mm).

## 3. Results and Discussion

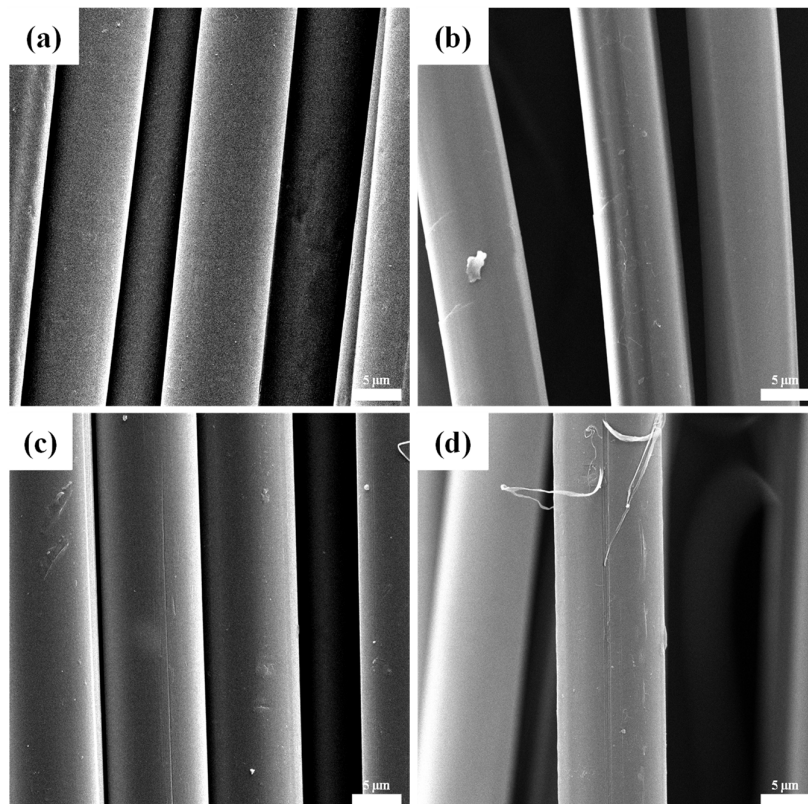
### 3.1. Influence of Phthalic Anhydride Solution Concentration on the Surface Properties of PPTA Fiber

#### 3.1.1. Study on Microstructures of PPTA Fiber Surface before and after Modification

PPTA fiber was modified with different concentrations of phthalic anhydride, with modification conditions as shown in Table 3. The surface morphology of aramid fiber before and after phthalic anhydride modification was observed using a Phenom Pro desktop scanning electron microscope (SEM), as shown in Figure 3. In Figure 3a, it can be observed that the surface of the unmodified PPTA fiber appears smooth. In Figure 3b, after modification with a solution of phthalic anhydride at a concentration of 0.15 mol/L (PPTA-0.15), the surface of the PPTA fiber shows a few protrusions and small grooves, indicating an increase in surface roughness. In Figure 3c, after modification with a solution of phthalic anhydride at a concentration of 0.30 mol/L (PPTA-0.30), there are more protruding structures, longer grooves, and stripes on the fiber surface. The protruding structures provide physical anchoring effects, while the grooves and stripes can increase the surface roughness and specific surface area of the PPTA-0.30 fiber. This enhances the degree of infiltration of the DGEBA matrix into the PPTA-0.30 fiber, strengthening the mechanical bonding at the interface of the composite material. In Figure 3d, after modification with 0.45 mol/L phthalic anhydride solution (PPTA-0.45), fiber delamination becomes more pronounced, indicating fiber fibrillation. This is attributed to the excessively high concentration of phthalic anhydride, which intensifies the degree of surface modification, leading to damage and detachment of the fiber cortex, and the detachment of the fiber cortex results in a decrease in the strength of the fiber itself.

**Table 3.** Phthalic anhydride modified fiber conditions.

Fiber Name	Fiber Modification Conditions
unmodified PPTA	unmodified
PPTA-0.15	0.15 mol/L phthalic anhydride + 80 °C + 2 h
PPTA-0.30	0.30 mol/L phthalic anhydride + 80 °C + 2 h
PPTA-0.45	0.45 mol/L phthalic anhydride + 80 °C + 2 h

**Figure 3.** SEM images of PPTA fiber surface before and after modification: (a) PPTA; (b) PPTA-0.15; (c) PPTA-0.3; (d) PPTA-0.45.

### 3.1.2. Study on Surface Element Compositions of Aramid Fiber before and after Modification

To investigate the reaction mechanism between phthalic anhydride and PPTA fiber, the surface elemental composition of PPTA fiber before and after modification were analyzed and compared. X-ray photoelectron spectroscopy (XPS) can determine the atomic bonding state and electron distribution state by measuring the chemical shift of a material's electronic spectrum, as well as identify atomic types and chemical states (excluding H, He) through the characteristic binding energies of the elements and the spectral lines in the XPS spectra. XPS is widely used for analyzing the surface modification of polymers.

Figure 4 shows the survey scan spectra of the surface chemical composition of PPTA fiber after modification with different concentrations of phthalic anhydride solutions. Figure 4a is the XPS survey scan spectrum of unmodified PPTA fiber, while Figure 4b, Figure 4c, and Figure 4d, respectively, represent the XPS survey scan spectrum of PPTA fiber after modification with 0.15 mol/L, 0.3 mol/L, and 0.45 mol/L phthalic anhydride solutions. In each survey scan spectrum, three strong peaks can be observed, corresponding to the presence of three elements on the surface of the PPTA fiber: carbon (C), nitrogen (N), and oxygen (O) elements. Furthermore, the relative content of the three elements can be quantitatively determined by the intensity of the peak. Comparing Figure 4a–c, with the increase in the concentration of phthalic anhydride, the C1s peak on the surface of PPTA

fiber shows a slight decrease, while the N1s and O1s peaks significantly increase. Especially after modification with a 0.3 mol/L solution of phthalic anhydride, the enhancement of the O1s peak is notably pronounced (Figure 4c). These changes indicate that after modification with phthalic anhydride solution, the oxygen content on the surface of PPTA fiber significantly increases; when the concentration of phthalic anhydride is in the range of 0~0.3 mol/L, the oxygen content on the fiber surface notably increases with the concentration, reaching its highest value at 0.3 mol/L. In Figure 4d, when the concentration of phthalic anhydride solution reaches 0.45 mol/L, the O1s peak decreases significantly and the O content drops sharply. This change indicates that the etching of the fiber surface is dominant at this time, leading to delamination of the fiber surface layer, causing the shedding of oxygen-containing functional groups and the decrease in oxygen content. The relative percentage contents of the three elements carbon (C), nitrogen (N), and oxygen (O) on the surface of PPTA fiber are shown in Table 4. The O/C ratios on the surface of unmodified PPTA fiber and PPTA fiber modified by 0.15 mol/L, 0.3 mol/L, and 0.45 mol/L phthalic anhydride solutions are 0.149, 0.156, 0.176, and 0.148, respectively. The data indicate that the optimal modification concentration for phthalic anhydride modified PPTA fiber is 0.3 mol/L. At this concentration, the most oxygen-containing functional groups are introduced into the fiber surface, the surface oxygen content is the highest, and the surface etching is relatively light. Below this concentration, the oxygen content is not ideal, while above this concentration, severe surface etching and delamination of the fiber occur.

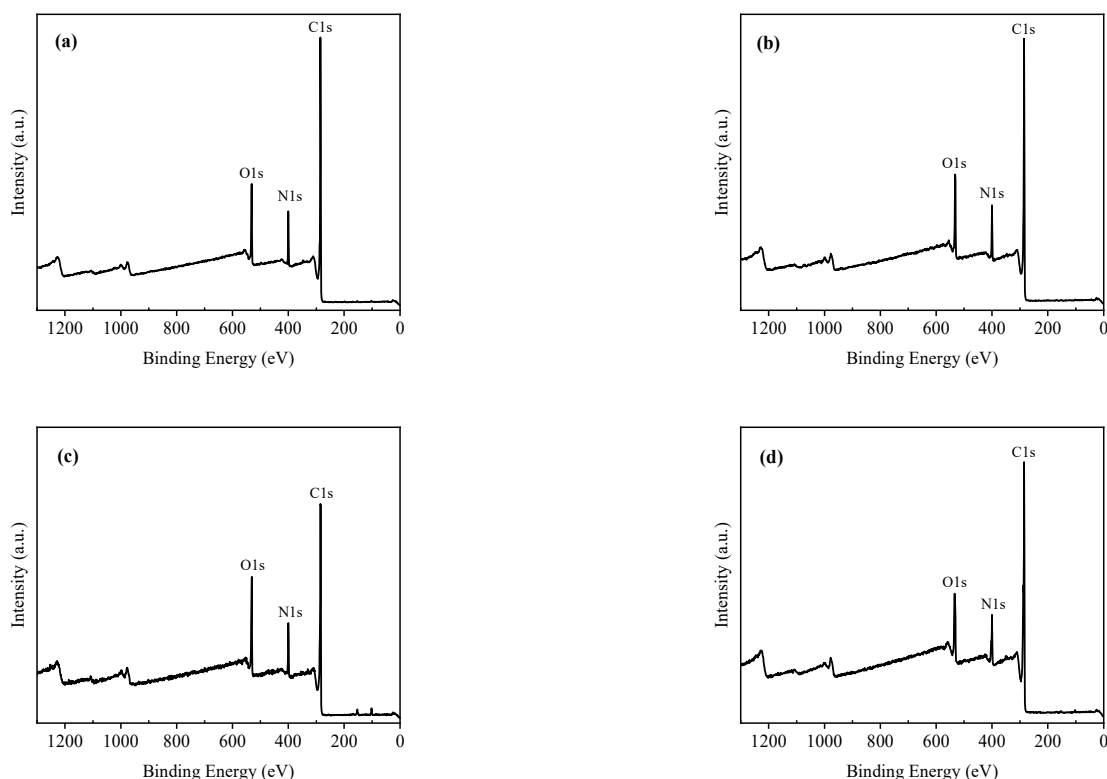


**Figure 4.** XPS full spectra of PPTA fiber before and after modification: (a) PPTA; (b) PPTA-0.15; (c) PPTA-0.3; (d) PPTA-0.45.

In order to further analyze the chemical states of surface elements on the PPTA fiber before and after modification, peak fitting was performed on the C1s spectrum, as shown in Figure 5. From Figure 5a, it can be observed that the functional groups on the unmodified PPTA fiber surface are mainly composed of C-C (284.5 eV), C-N (285.5 eV), and C=O (287.7 eV). After modification with phthalic anhydride, new functional groups, such as C-O (286.3 eV) and O=C-O (289.9 eV), were introduced onto the PPTA fiber surface, resulting in increased oxygen content and a higher proportion of polar oxygen-containing functional

groups. This change enhances the chemical bonding strength between PPTA fibers and the DGEBA matrix and improves the wettability and adhesion property of the PPTA fiber surfaces, thereby enhancing the interfacial bonding strength in the PPTA fiber-reinforced composite materials.

**Table 4.** Surface element content of PPTA fibers before and after modification.

Fiber Name	Surface Element Content			Element Ratio O/C
	C	N	O	
unmodified PPTA	79.02	9.21	11.77	0.149
PPTA-0.15	78.32	9.45	12.23	0.156
PPTA-0.30	76.58	9.93	13.49	0.176
PPTA-0.15	78.58	9.78	11.64	0.148

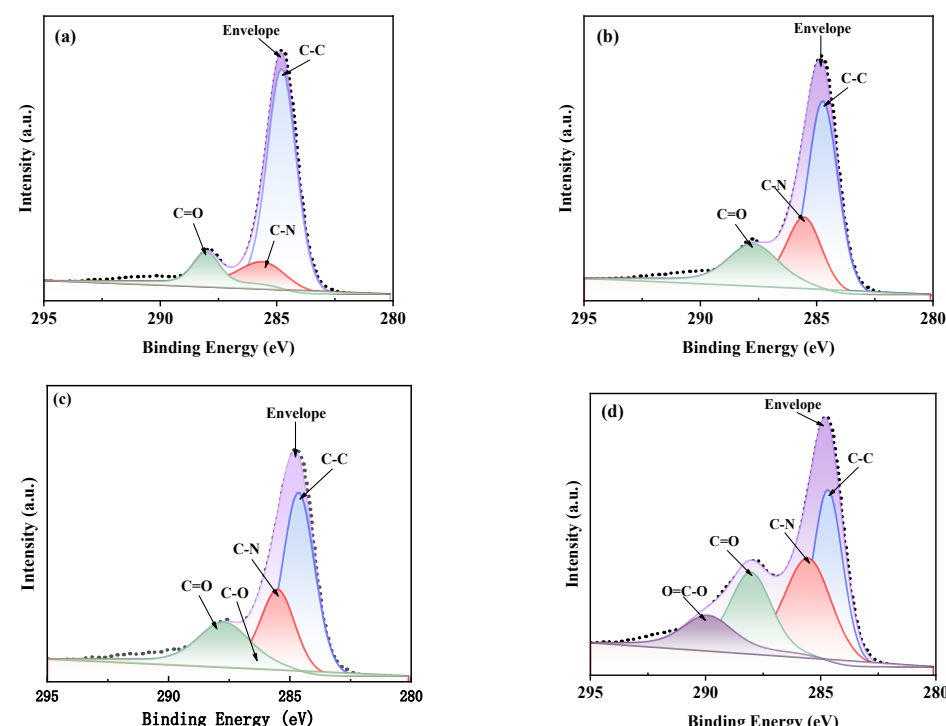


**Figure 5.** C1s spectra of PPTA fibers before and after modification: (a) PPTA; (b) PPTA-0.15; (c) PPTA-0.3; (d) PPTA-0.45.

### 3.1.3. Study on Crystalline Structures of Aramid Fibers before and after Modification

X-ray diffraction (XRD) was used to analyze the changes in the crystal structure of the PPTA fiber before and after modification. The molecular structure segments of the cortex of PPTA fiber are arranged in a highly regular manner, exhibiting high crystallinity and orientation. Figure 6 shows the XRD diagram of the PPTA fiber after modification with different concentrations of phthalic anhydride solution. From the figure, the PPTA fiber has three obvious characteristic diffraction peaks at  $2\theta = 20.7^\circ$ ,  $22.9^\circ$ , and  $29.0^\circ$ . These are the characteristic peaks of PPTA fiber, corresponding to the (110), (200), and (004) crystal planes of PPTA fiber, respectively; after modification with 0.15 mol/L and 0.3 mol/L concentrations of phthalic anhydride solution, the three characteristic diffraction peaks of the fiber show no significant changes, indicating that the fiber structure remains unaffected. However, when the concentration of phthalic anhydride solution increases to 0.45 mol/L, the diffraction peaks of the fibers broaden, and the two main peaks at  $2\theta = 20.7^\circ$  and  $22.9^\circ$  are weakened, indicating that at this point, the surface etching effect on the fiber is too strong, leading to delamination of the fiber cortex and a decrease in crystallinity.

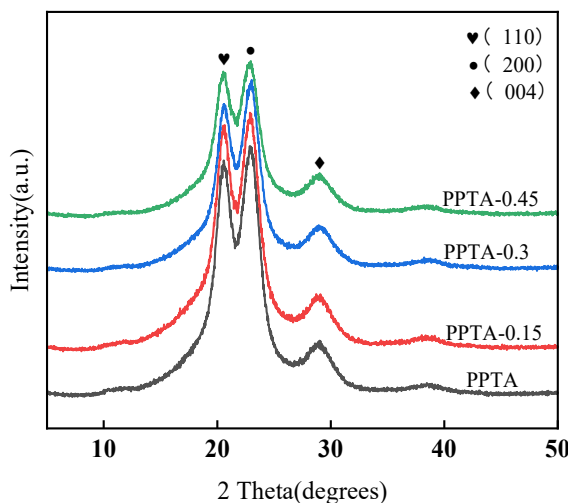


**Figure 6.** XRD diagram of PPTA fiber before and after modification.

### 3.2. Influence of Anhydrous $\text{AlCl}_3$ Catalysis Modification Time on Surface Properties of PPTA Fiber

#### 3.2.1. SEM Analysis of Fiber Surface Morphology before and after Modification

To further investigate the influence of catalytic modification with anhydrous  $\text{AlCl}_3$  on the properties of fibers, PPTA fibers were treated with a 0.3 mol/L solution of phthalic anhydride under the catalytic effect of anhydrous  $\text{AlCl}_3$  for different durations (0.5 h, 1 h, 1.5 h, and 2 h).

The modification conditions for each fiber are shown in Table 5. For the PPTA-2h fiber, its modification process is identical to that of the PPTA-0.3 fiber. To explore the impact of the catalytic modification time on both the fibers and the composite materials, we named the PPTA-0.3 fiber “PPTA-2h” to indicate its association with time. Under the catalysis of anhydrous  $\text{AlCl}_3$ , the SEM images of PPTA fiber treated with different time of modification are shown in Figure 7. As previously analyzed, the surface of the unmodified PPTA fiber is smooth and defect-free (Figure 3a); after 2 h of modification, the surface of the PPTA fiber exhibits protrusions and grooves (Figure 3c). In Figure 7a, for PPTA-0.5 h (A), there are more protrusions, grooves, and stripes on the fiber surface, indicating an increased roughness; in Figure 7b, for PPTA-1 h (A), there are more protrusions and small grooves on the fiber surface, leading to an increased roughness. Additionally, detached microfibers can be observed on the fiber surface at this point, indicating damage to the fibers; in Figure 7c, for PPTA-1.5 h (A), delamination occurs in the cortex layer due to prolonged modification time. The excessive modification causes damage to the fiber surface and reduces its overall strength. Finally, in Figure 7d, for PPTA-2 h (A), there is a greater degree of delamination on the fibers surface with an increase in both quantity and width of microfibers at these detachment sites.

**Table 5.** Catalytic modification conditions of anhydrous  $\text{AlCl}_3$ .

Fiber Name	Fiber Modification Conditions
unmodified PPTA	unmodified
PPTA-2 h	0.30 mol/L phthalic anhydride + 80 °C + 2 h
PPTA-0.5 h (A)	0.3 mol/L phthalic anhydride + anhydrous $\text{AlCl}_3$ + 80 °C + 0.5 h
PPTA-1 h (A)	0.3 mol/L phthalic anhydride + anhydrous $\text{AlCl}_3$ + 80 °C + 1 h
PPTA-1.5 h (A)	0.3 mol/L phthalic anhydride + anhydrous $\text{AlCl}_3$ + 80 °C + 1.5 h
PPTA-2 h (A)	0.3 mol/L phthalic anhydride + anhydrous $\text{AlCl}_3$ + 80 °C + 2 h

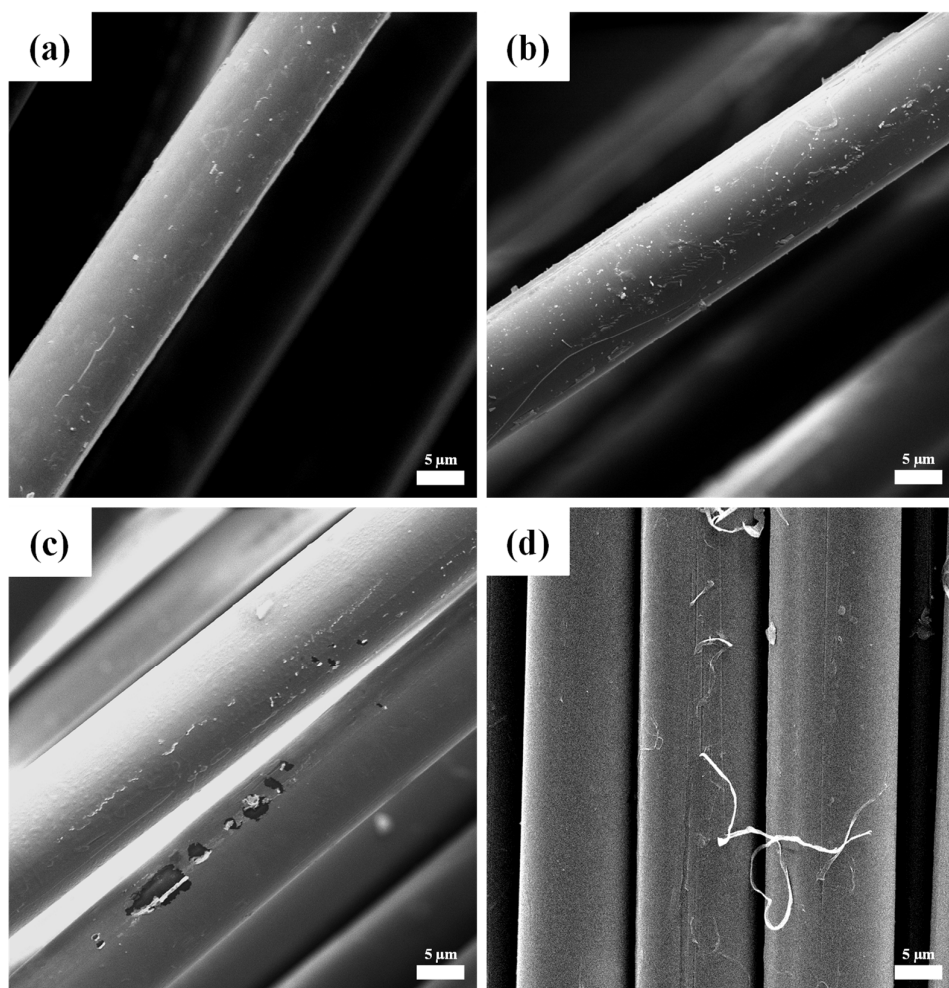


**Figure 7.** SEM images of PPTA fiber surface at different times of catalytic modification: (a) PPTA-0.5 h (A); (b) PPTA-1 h (A); (c) PPTA-1.5 h (A); (d) PPTA-2 h (A).

### 3.2.2. Analysis of AFM on Surface Morphology of Fibers before and after Modification

Atomic force microscopy (AFM) is widely used to observe the nanoscale morphology of sample surfaces, with a resolution that can reach the atomic level. Table 6 shows the average surface roughness of the PPTA fiber before and after modification, and Figure 8 presents AFM images of the PPTA fiber before and after modification. For unmodified PPTA fibers, the surface is smooth, without prominent protrusions or indentations, and exhibits low surface roughness (Figure 8a). After modification with phthalic anhydride for 2 h (PPTA-2 h), the surface of the fibers exhibits obvious protrusions and grooves (Figure 8b), resulting in an increase in the fiber surface Ra value. For catalytic modification, the surface roughness and height of the PPTA-0.5 h (A) fibers increase (Figure 8c), leading to a further increase in the Ra value. This is consistent with the SEM analysis and indicates that catalytic modification, while saving time, can further etch the fiber surface, increase surface roughness, enhance mechanical interlocking between fibers and resins, and improve the bonding strength of the composite material interfaces.

**Table 6.** Average surface roughness of PPTA fiber before and after catalytic modification.

Fiber	Unmodified PPTA	PPTA-2 h	PPTA-0.5 h (A)
$R_a$ (nm)	0.10	0.59	1.31

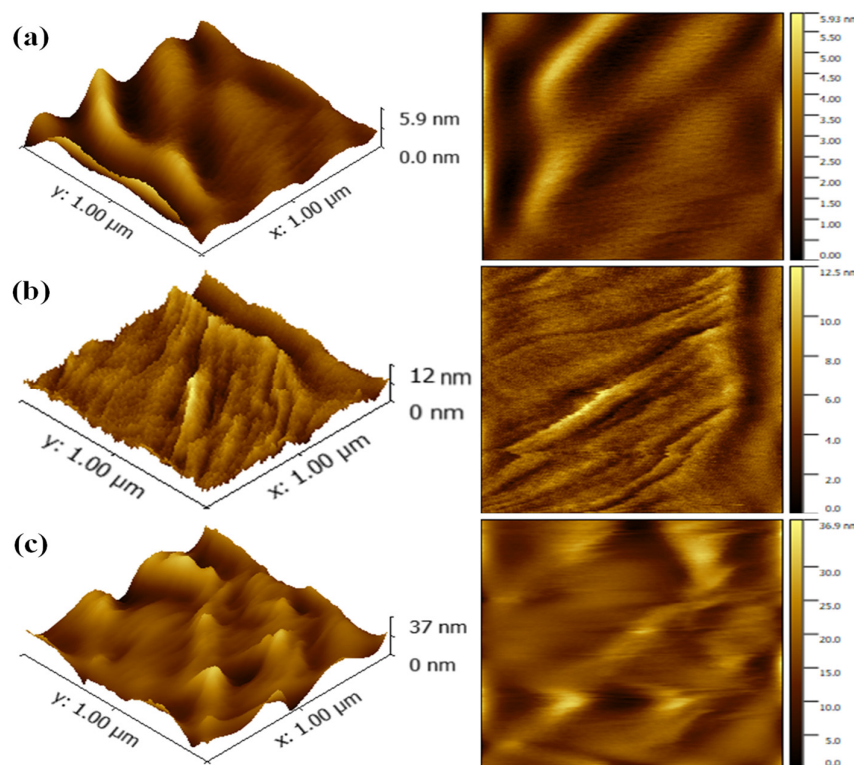


**Figure 8.** AFM diagram of PPTA fiber before and after catalytic modification: (a) PPTA; (b) PPTA-2 h; (c) PPTA-0.5 h (A).

### 3.2.3. Study of Surface Elemental Composition before and after Catalytic Modification of Fiber

To investigate the catalytic mechanism of anhydrous  $\text{AlCl}_3$ , surface elemental analysis was conducted on unmodified PPTA fiber, uncatalytic modified PPTA-2 h fiber, and fiber modified with different durations under catalytic conditions. Figure 9 shows the XPS full spectra of the fibers before and after modification. Figure 9a depicts unmodified PPTA fiber, while Figure 9b shows PPTA-2 h fiber modified with 0.3 mol/L phthalic anhydride for 2 h. Figures 9c, 9d, 9e and 9f, respectively, illustrate PPTA-0.5 h (A), PPTA-1 h (A), PPTA-1.5 h (A), and PPTA-2 h (A) fibers modified with 0.3 mol/L phthalic anhydride for 0.5, 1, 1.5, and 2 h under catalytic conditions with anhydrous  $\text{AlCl}_3$ . From Figure 9a, it can be observed that the surface of unmodified PPTA fiber mainly consists of three elements, C, N, and O, which are consistent with its molecular composition. In Figure 9, the C1s peak and N1s peak of the catalytically modified fibers are lower compared to those of unmodified PPTA fiber and PPTA-2 h fiber, while the O1s peak is significantly enhanced. Relative percentages of the three elements were calculated using Avantage 5.9931 software, and the results are presented in Table 7. The surface element O/C ratios of PPTA-0.5 h (A) fiber, PPTA-1 h (A) fiber, PPTA-1.5 h (A) fiber, and PPTA-2 h (A) fiber are 0.307, 0.389, 0.355, and 0.318, respectively, nearly twice as high as those of unmodified PPTA fiber and PPTA-2 h fiber. This indicates that the addition of the catalyst anhydrous  $\text{AlCl}_3$  in the modification process accelerates the reaction rate, increases the reaction extent, introduces more polar oxygen-containing functional groups on the fiber surface, and enhances the oxygen content on the fiber surface. However, if the catalytic modification time is too long (1.5 h, 2 h), the excessive etching effect will exacerbate the degree of fiber surface delamination and the loss of polar oxygen-containing functional groups, leading to a decrease in the relative oxygen content.

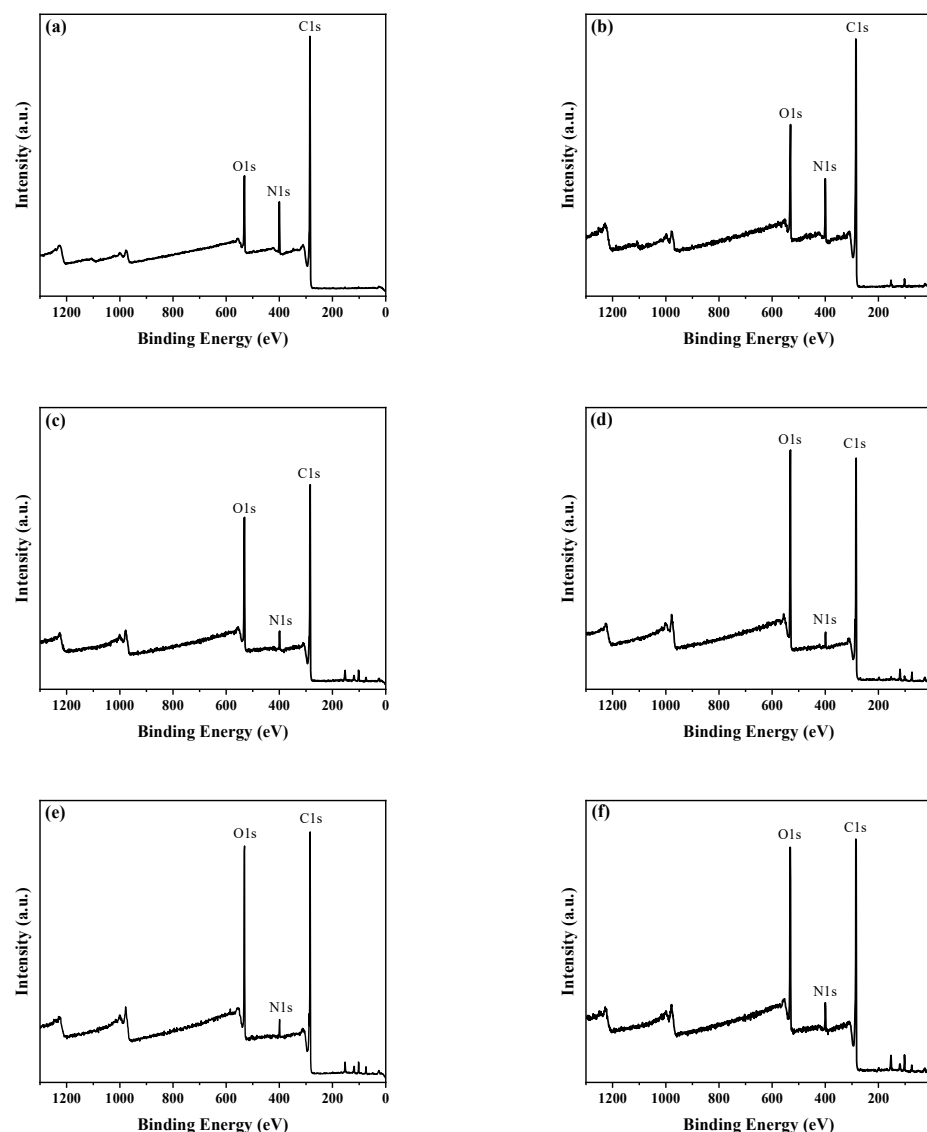


**Figure 9.** XPS full spectrum of PPTA fiber before and after catalytic modification: (a) PPTA; (b) PPTA-2 h; (c) PPTA-0.5 h (A); (d) PPTA-1 h (A); (e) PPTA-1.5 h (A); (f) PPTA-2 h (A).

**Table 7.** Surface element content of PPTA fiber before and after modification.

Fiber Name	Surface Element Content			Element Ratio O/C
	C	N	O	
unmodified PPTA	79.02	9.21	11.77	0.149
PPTA-2 h	76.58	9.93	13.49	0.176
PPTA-0.5 h (A)	73.01	4.61	22.38	0.307
PPTA-1 h (A)	70.01	2.75	27.24	0.389
PPTA-1.5 h (A)	70.83	4.05	25.12	0.355
PPTA-2 h (A)	70.53	7.02	22.45	0.318

To further analyze the changes in the surface functional groups of the PPTA fiber during catalytic modification and investigate the chemical reaction mechanism occurring on the fiber surface during this process, peak fitting of the C1s peak was performed using Avantage software, and the results are shown in Figure 10. In Figure 10a, the surface functional groups of unmodified PPTA fiber mainly include C-C (284.5 eV), C-N (285.5 eV), and C=O (287.7 eV). In Figure 10b, C-O (286.3 eV) is introduced on the

surface of PPTA-2 h fiber. From Figure 10c–f, it can be observed that the types of polar oxygen-containing functional groups introduced on the fiber surface remain unchanged after catalytic modification, but the number of polar oxygen-containing functional groups increases. This indicates that the catalyst anhydrous  $\text{AlCl}_3$  can increase the reaction rate, improve the reaction yield, enhance the chemical bonding and wetting properties between the fiber and the matrix, and improve the interfacial bonding of fiber-reinforced resin matrix composites.

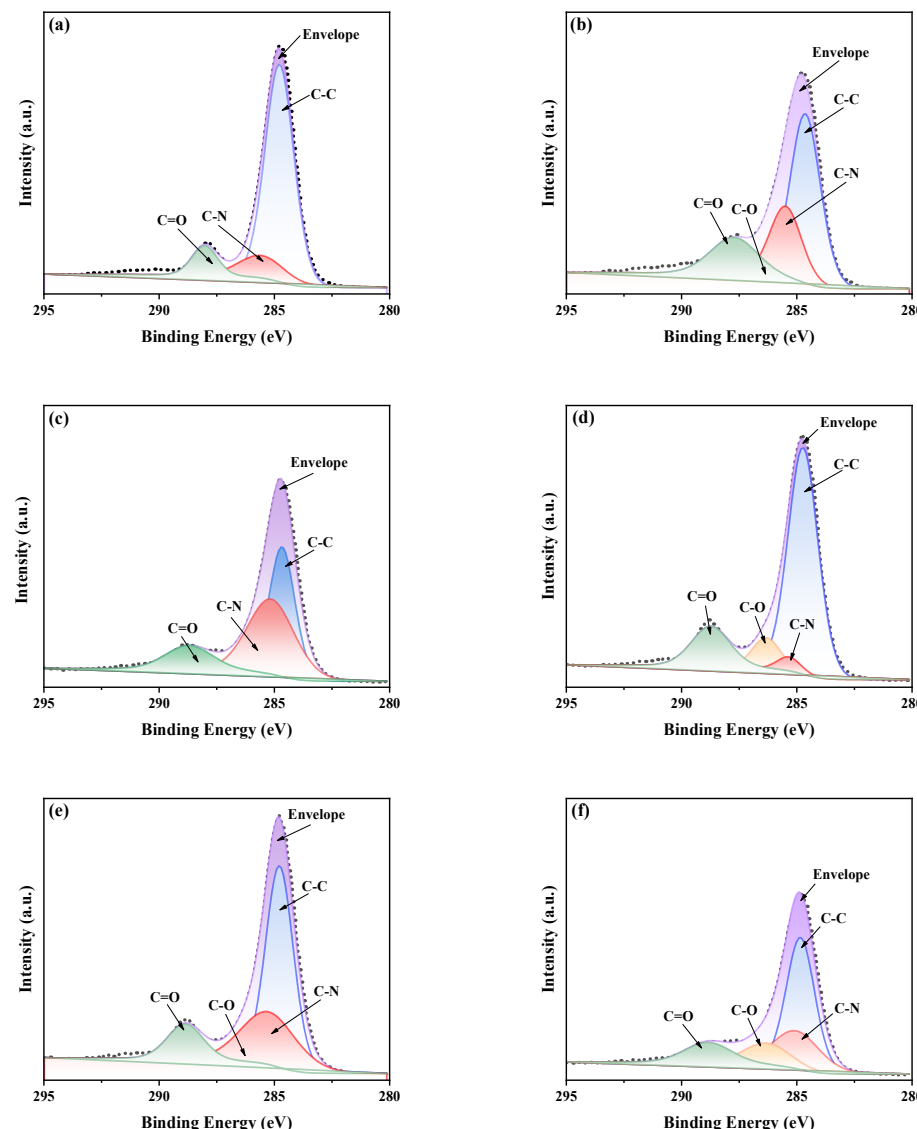


**Figure 10.** C1s spectra of PPTA fiber before and after catalytic modification: (a) PPTA; (b) PPTA-2 h; (c) PPTA-0.5 h (A); (d) PPTA-1 h (A); (e) PPTA-1.5 h (A); (f) PPTA-2 h (A).

### 3.2.4. Fiber Crystal Structures before and after Catalytic Modification

Figure 11 depicts the XRD patterns of PPTA fiber after modification. Compared to PPTA-2 h fiber, there is no significant change observed in the diffraction peaks of PPTA-0.5 h (A) fiber and PPTA-1 h (A) fiber after catalytic modification, indicating that the aggregate structure of fibers remains unchanged and no new crystalline structure is formed after catalytic modification, which mainly occurs on the surface of the fibers. The position and range of the diffraction peaks of PPTA-1.5 h (A) fiber also show no significant change, suggesting that the crystalline structure of PPTA-1.5 h (A) fiber remains unchanged. However, the intensity of the two major diffraction peaks of PPTA-1.5 h (A) fiber noticeably

decreases, indicating that the chemical composition and structure of the fiber surface are affected. Prolonged catalytic modification leads to increased surface etching of fiber, causing the detachment of highly crystalline outer layers, thereby reducing the overall crystallinity of fiber. The broadening of diffraction peaks for PPTA-2 h (A) fiber suggests that prolonged etching continuously leads to surface peeling, resulting in a continuous decrease in fiber crystallinity, which can compromise the intrinsic strength of the fiber. Therefore, it is necessary to control the duration of catalytic modification; excessive modification time (1.5 h, 2 h) may decrease the intrinsic strength of the fiber.

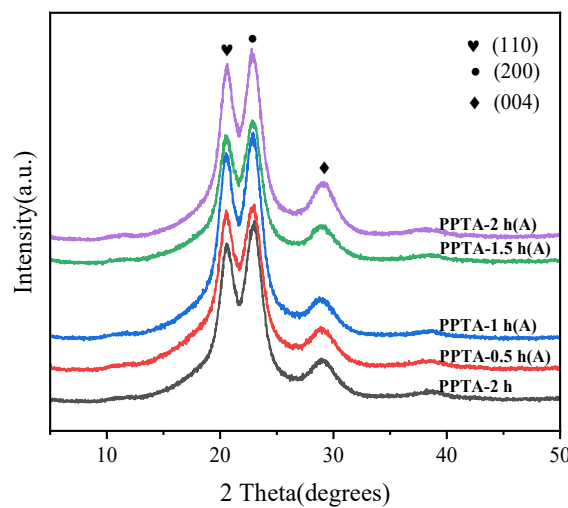


**Figure 11.** XRD diagram of catalytic modified PPTA fiber.

### 3.3. Influence of Modification Treatment on Properties of PPTA/DGEBA Composite Materials

#### 3.3.1. Interfacial Properties of PPTA/DGEBA Composites before and after Anhydride Modification

The PPTA fiber modified by phthalic anhydride solution of different concentrations was hot pressed with DGEBA to prepare the PPTA/DGEBA composite material. The interlaminar shear strength is shown in Figure 12; the interlaminar shear strength of the modified PPTA composites is higher than that of the unmodified PPTA composites. Specifically, the interlaminar shear strengths of the unmodified PPTA, PPTA-0.15, PPTA-0.30, and PPTA-0.45 composites are 10.79 MPa, 11.65 MPa, 12.51 MPa, and 12.20 MPa, respectively. The interlaminar shear strength of the PPTA-0.30 composite is 15.94% higher than that of the unmodified PPTA composite, indicating that the PPTA fiber modified with a 0.30 mol/L phthalic anhydride solution and then combined with DGEBA exhibits the highest interlaminar shear strength. The optimal treatment concentration for modifying PPTA fiber with phthalic anhydride solution is 0.30 mol/L.

The interaction mechanism studied herein between the fibers and matrix is interface modification [47]. The mechanism involves introducing chemical functional groups onto the fiber surface through chemical treatment to enhance the adhesion and compatibility between the fiber and matrix [48]. As the chemical treatment progresses, it creates chemical active sites on the fiber surface, forming strong bonds with chemical groups in the matrix, thereby increasing the adhesion strength of the interface. However, with further treatment, more severe fiber etching occurs, adversely affecting the properties of the fibers themselves, resulting in a decrease in interface performance.

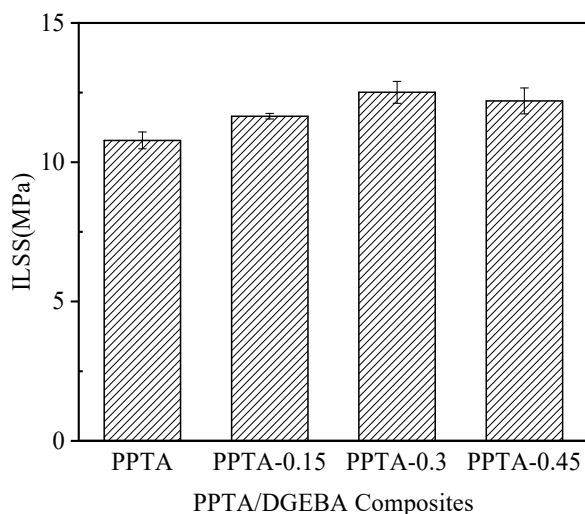


**Figure 12.** Interlaminar shear strength of PPTA/DGEBA composites before and after anhydride modification.

### 3.3.2. Interfacial Properties of PPTA/DGEBA Composite Materials before and after Catalytic Modification

The interlaminar shear strength of PPTA/DGEBA composite materials before and after catalytic modification of phthalic anhydride by anhydrous  $\text{AlCl}_3$  is shown in Figure 13. The interlaminar shear strength of the unmodified PPTA samples is 10.79 MPa. After modification, the interlaminar shear strength of the PPTA-2 h samples increases to 12.51 MPa. For the catalytically modified PPTA-0.5 h(A), PPTA-1 h(A), PPTA-1.5 h(A), and PPTA-2 h(A) samples, the interlaminar shear strengths are 16.15 MPa, 14.15 MPa, 13.71 MPa, and 13.03 MPa, respectively. Among them, the interlaminar shear strength of the PPTA-0.5 h(A) samples is increased by 49.68% compared to the unmodified PPTA samples and by 29.10% compared to the PPTA-2 h samples.

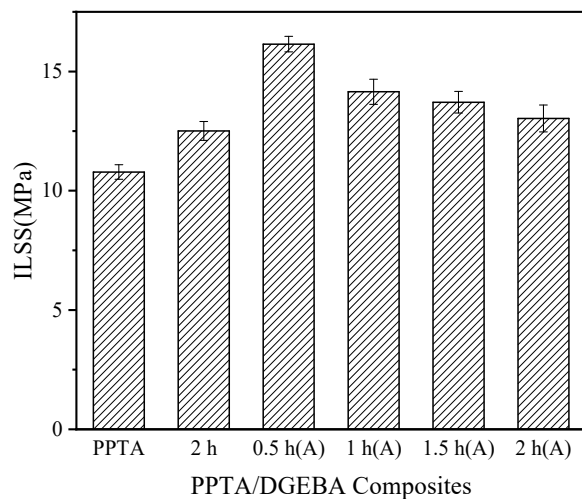


**Figure 13.** Interlaminar shear strengths of PPTA/DGEBA composites before and after catalytic modification.

Combining the previous analysis of the microstructure and elemental composition of the PPTA fiber surfaces before and after modification, it is evident that the addition of the catalyst anhydrous  $\text{AlCl}_3$  during modification introduces more polar oxygen-containing functional groups on the fiber surface. These polar functional groups form chemical bonds with the DGEBA matrix, thereby improving interfacial adhesion and bond strength. Additionally, the formation of “protrusions,” small grooves, and stripes on the fiber surface

enhances physical anchoring, strengthening the mechanical interlocking between the fiber and the matrix. Moreover, these “protrusions,” grooves, and stripes increase the specific surface area of fibers, thereby increasing the free energy of the fiber surface. This facilitates better spreading of the matrix on the fiber surface, improving wettability, and enhancing interfacial adhesion. Among these, the interlaminar shear strength of the PPTA-0.5 h (A) sample shows the most significant improvement, indicating optimal modification effects on its fibers and optimal interfacial bonding performance of the composite material.

### 3.3.3. Mechanical Properties of PPTA/DGEBA Composite Materials before and after Maleic Anhydride Modification

The tensile strength and flexural strength of the PPTA/DGEBA composite materials after modification with different concentrations of phthalic anhydride are shown in Figure 14. The tensile strength of the unmodified PPTA specimens is 196.64 MPa. For the PPTA-0.15 specimens, the tensile strength is 208.91 MPa, while for the PPTA-0.3 specimens, it is 231.91 MPa, representing an increase of 17.94% compared to the unmodified PPTA specimens. The tensile strength of the PPTA-0.45 specimens is 177.55 MPa. The flexural strength of the modified composite materials is higher than that of the unmodified composite materials. The flexural strength of the unmodified PPTA specimens is 138.27 MPa, while for the PPTA-0.15 specimens, it is 154.01 MPa. The PPTA-0.3 specimens exhibit a flexural strength of 199.36 MPa, representing a 44.18% increase compared to the unmodified PPTA specimens. The flexural strength of the PPTA-0.45 specimens is 145.44 MPa.

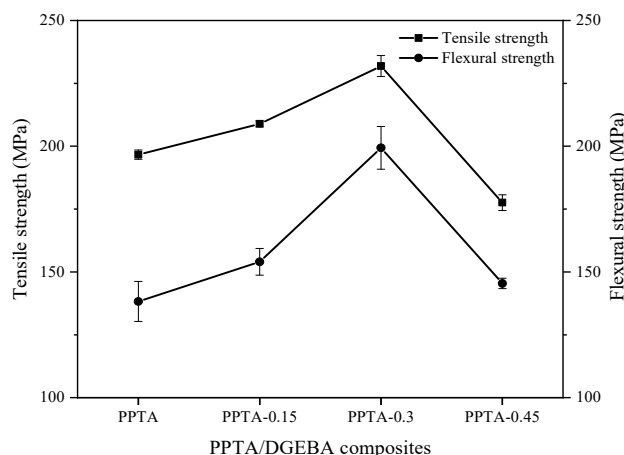


**Figure 14.** Tensile strength and flexural strength of PPTA/DGEBA composites before and after modification.

With an increase in the concentration of phthalic anhydride, the mechanical properties of the PPTA/DGEBA composite materials exhibit a trend of initially increasing and then decreasing. When the concentration of phthalic anhydride is 0.3 mol/L, the mechanical properties of the PPTA/DGEBA composite materials reach their optimum. This is attributed to the modification of PPTA fibers by phthalic anhydride, which can increase the surface roughness and polarity functional groups of the fibers, thereby enhancing the mechanical interlocking and chemical bonding between the fibers and the resin matrix. Consequently, within the concentration range of 0 to 0.3 mol/L of phthalic anhydride, the mechanical properties of the PPTA/DGEBA composite materials are strengthened with increasing concentration of phthalic anhydride. However, when the concentration of phthalic anhydride exceeds 0.3 mol/L, the surface etching of the fibers intensifies, and the fiber coating begins to peel off, resulting in a decrease in the intrinsic strength of the fibers. Since the outstanding performance of the fibers as reinforcing agents cannot be fully realized, the mechanical properties of the composite material exhibit a decreasing trend within the concentration range of 0.3 to 0.45 mol/L of phthalic anhydride.

### 3.3.4. Mechanical Properties of PPTA/DGEBA Composite Materials before and after Catalytic Modification

The tensile strength of PPTA/DGEBA composite materials before and after catalytic modification of PPTA fiber is shown in Figure 15a. The stress–strain curves during the tensile process of PPTA/DGEBA composite materials before and after catalytic modification are shown in Figure 15b. In Figure 15a, the tensile strength of the unmodified PPTA samples is 196.64 MPa, while that of the PPTA-2 h samples is 231.91 MPa. The tensile strength of the PPTA-0.5 h (A) samples is 306.77 MPa, which is 32.28% higher than that of the PPTA-2 h samples and 56.01% higher than that of the unmodified PPTA samples. With increase in the catalytic modification time, the tensile strength of the composite materials decreases. The tensile strengths of samples modified for 1 h, 1.5 h, and 2 h are 241.40 MPa, 153.97 MPa, and 138.57 MPa, respectively. The flexural strength of the unmodified PPTA samples is 138.27 MPa, while that of the PPTA-2 h samples is 199.31 MPa. The flexural strengths of the PPTA-0.5 h (A), PPTA-1 h (A), PPTA-1.5 h (A), and PPTA-2 h (A) samples are 248.95 MPa, 232.12 MPa, 160.66 MPa, and 147.12 MPa, respectively. Among them, the flexural strength of the PPTA-0.5 h(A) samples is 24.91% higher than that of the PPTA-2 h samples.

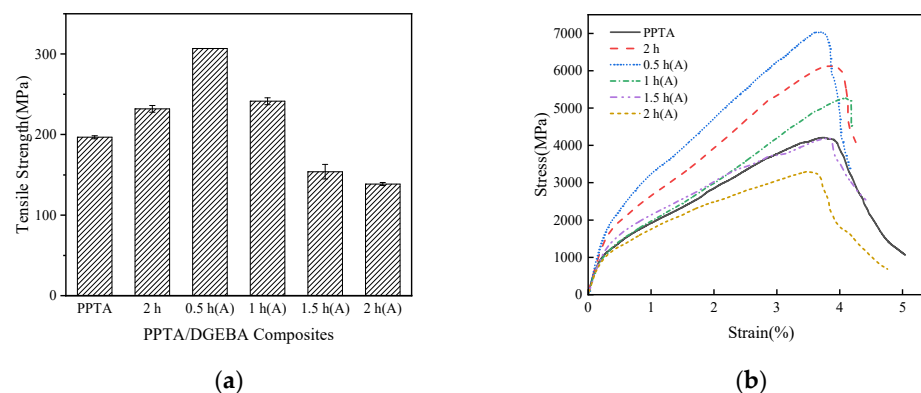


**Figure 15.** (a) Tensile strength of PPTA/DGEBA composites; (b) PPTA/DGEBA stress–strain curve during tensile process.

Figure 15b depicts the stress–strain curves of the PPTA/DGEBA composite materials before and after catalytic modification during tensile testing. Initially, when subjected to axial tensile loading, the composite material mainly bears the load through the DGEBA matrix. As the tensile displacement increases, both the fiber and matrix, as well as their interfacial adhesion, collectively bear the load. Due to the lower toughness of the resin matrix compared to the fiber reinforcement, matrix fracture begins to occur, corresponding to the inflection point on the curve where the slope gradually decreases. After catalytic modification, the increased presence of polar oxygen-containing functional groups on the surface of PPTA-0.5 h (A) fibers significantly enhances the adhesion between the fiber and matrix, resulting in an increase in stress at the inflection point of the stress–strain curve. However, excessively prolonged catalytic modification time (PPTA-1 h (A), PPTA-1.5 h (A), PPTA-2 h (A)) exacerbates surface erosion of the fiber, leading to potential detachment of the fiber's surface layer and a decrease in the intrinsic strength of the fiber. Consequently, the interfacial adhesion between the fiber and resin cannot be improved, resulting in a decrease in stress at the inflection point and a reduction in tensile performance of the composite material. As the tensile displacement continues to increase, DGEBA matrix failure occurs, and the tensile load is primarily borne by the fiber reinforcement until the sample is damaged, reaching its maximum tensile strength.

The flexural strength of the PPTA/DGEBA composite materials before and after catalytic modification of PPTA fiber is shown in Figure 16a. The stress–strain curves during the bending process of the PPTA/DGEBA composite materials before and after catalytic modification are shown in Figure 16b. In Figure 16a, the flexural strength of the unmodified

PPTA samples is 138.27 MPa, while that of the PPTA-2 h samples is 199.31 MPa. The flexural strengths of the PPTA-0.5 h (A), PPTA-1 h (A), PPTA-1.5 h (A), and PPTA-2 h (A) samples are 248.95 MPa, 232.12 MPa, 160.66 MPa, and 147.12 MPa, respectively. Among them, the flexural strength of the PPTA-0.5 h (A) samples is 24.91% higher than that of the PPTA-2 h samples. The flexural performance of the PPTA/DGEBA composite material is significantly improved after catalytic modification.

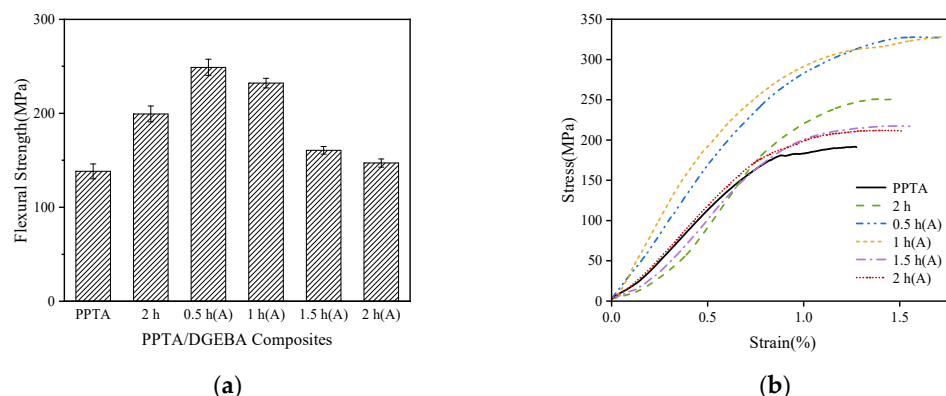


**Figure 16.** (a) Flexural strength of PPTA/DGEBA composites; (b) PPTA/DGEBA stress–strain curve during flexural process.

In Figure 16b, it can be observed that the peaks of the stress–strain curves for all specimens exhibit an arc shape, and the increase in load after reaching the peak gradually decreases with increasing displacement. During the bending failure process, the failure modes of the PPTA/DGEBA composite material include compression failure in the upper layer, shear failure in the middle layer, tensile failure in the lower layer, and delamination. The compression strain of the PPTA/DGEBA composite material is four times that of the tensile strain, but its compression strength is only one-fourth of the tensile strength. Therefore, in bending tests, the PPTA fiber on the compression side will exhibit a “yielding” phenomenon at low strains under load, manifested as a turning point appearing before the peak on the stress–strain curve. At this point, the entire PPTA/DGEBA specimen still has a significant load-carrying capacity, eventually forming an arc-shaped peak in the stress–strain curve. A slight fluctuation can be observed on the stress–strain curve of the unmodified PPTA specimen, which is due to the occurrence of fracture in the DGEBA matrix at that time. Through data comparison, it was found that the order of bending stress magnitude for the specimens is as follows: PPTA-0.5 h (A) > PPTA-1 h (A) > PPTA-2 h > PPTA-1.5 h (A) > PPTA-2 h (A) > PPTA.

Combining the analysis of the microstructure and element composition of the fiber surfaces before and after modification, the catalytic action of anhydrous  $\text{AlCl}_3$  increases the number of polar functional groups on the fiber surface and increases surface roughness. This enhancement strengthens the chemical bonding and mechanical interlocking between the fiber and the DGEBA matrix, thereby improving the interfacial adhesion and tensile strength of the PPTA/DGEBA composite material. However, prolonged modification can lead to fiber damage and surface layer detachment, resulting in a decrease in intrinsic strength. Consequently, the excellent properties of the fibers as reinforcing agents are not fully utilized, thereby negatively affecting the tensile performance of the composite material.

Figure 17 depicts the side-view micrographs of the PPTA/DGEBA composite materials after bending failure at different catalytic modification times. In Figure 17a,b, at the interface delamination after bending failure, both the PPTA-0.5 h (A) fibers and the PPTA-1 h (A) fibers are encapsulated by resin, with multiple fibers bonded together through resin, collectively sharing the bending load. Additionally, good interfacial adhesion effectively transfers stress, significantly enhancing the bending strength of the composite material.

However, in Figure 17c, fiber fracture is evident due to prolonged catalytic modification of 1.5 h, causing surface delamination and detachment of fibers, resulting in structural damage to the fibers and leading to fracture failure under load, consequently reducing the bending strength of the composite material. In Figure 17d, fiber fracture is similarly observed, with less resin attached to the fiber surface, indicating exacerbated surface etching of fibers due to prolonged 2 h catalytic modification, resulting in severe fiber damage and another decrease in the bending strength of the composite material.

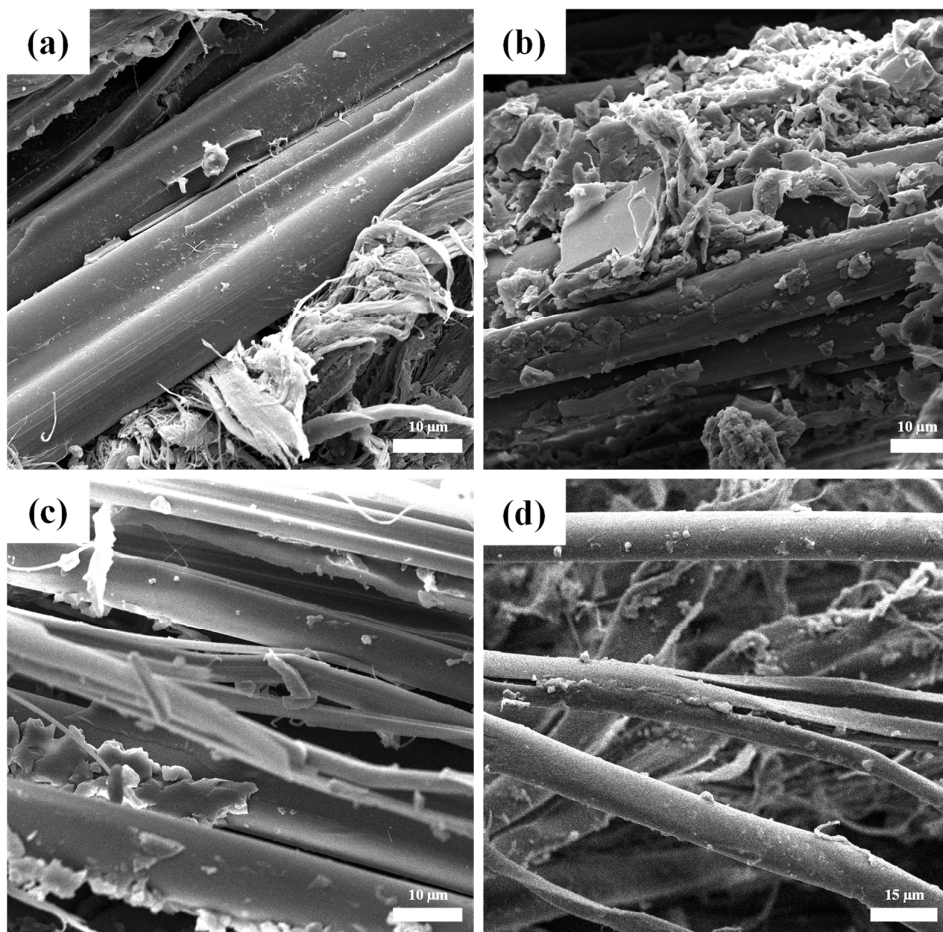


**Figure 17.** Lateral microscopic morphology of catalytically modified PPTA/DGEBA composites after bending damage: (a) PPTA-0.5h (A); (b) PPTA-1 h (A); (c) PPTA-1.5 h (A); (d) PPTA-2 h (A).

#### 4. Conclusions

1. Phthalic anhydride can undergo an acylation reaction with PPTA fiber, introducing -OH active functional groups onto the phenyl rings of the fibers. Some of the amide bonds on the fibers undergo hydrolysis to form -COOH, increasing the O/C elemental ratio on the fiber surface. With increase in the concentration of phthalic anhydride, the O/C ratio initially increases and then decreases. When the concentration of pyromellitic anhydride is 0.3 mol/L, the O/C ratio reaches its maximum value of 0.176, representing an 18.12% increase compared to unmodified PPTA fiber.
2. After modification with 0.3 mol/L phthalic anhydride, the tensile strength, flexural strength, and interlaminar shear strength of the PPTA/DGEBA composite materials all increased to their maximum values, showing improvements of 17.94%, 44.18%, and 15.94%, respectively, compared to unmodified specimens.
3. Anhydrous AlCl<sub>3</sub> can serve as a catalyst for the acylation reaction between phthalic anhydride and PPTA fiber, reducing the modification time and increasing the introduction rate of oxygen-containing functional groups on the fiber surface, resulting

in an increase in the O/C elemental ratio on the fiber surface. After catalytic modification for 0.5 h, 1 h, 1.5 h, and 2 h, the O/C elemental ratio on the fiber surface shows an increasing trend. Compared to PPTA fiber modified without the addition of catalyst, the O/C elemental ratio increased by 74.43%, 121.02%, 101.70%, and 80.68%, respectively.

4. After catalytic modification for 0.5 h, the tensile strength, flexural strength, and interlaminar shear strength of the PPTA/DGEBA composite materials all increased to their maximum values. Compared to non-catalyzed modified samples, there were improvements of 32.28%, 24.91%, and 29.10%, respectively.

**Author Contributions:** Conceptualization, Y.X. and X.Q.; methodology, Y.X. and Y.E.; investigation, Y.E. and G.X.; data curation, H.G. and H.L.; writing—original draft preparation, Y.E. and Y.X.; writing—review and editing, Y.X.; supervision, X.Q.; project administration, Y.X. and X.Q.; funding acquisition, Y.X. All authors have read and agreed to the published version of the manuscript.

**Funding:** This work was funded by the Defence Science and Technology Base Strengthening Programme of China and the China Construction Corporation Technology R&D Plan (CSCEC-2020-Z-1).

**Institutional Review Board Statement:** Not applicable.

**Informed Consent Statement:** Not applicable.

**Data Availability Statement:** Not applicable.

**Acknowledgments:** The authors gratefully acknowledge the financial support provided by the Defence Science and Technology Base Strengthening Programme of China and the China Construction Corporation Technology R&D Plan (CSCEC-2020-Z-1, CSCEC-2022-Z-8).

**Conflicts of Interest:** The authors declare no conflicts of interest.

## References

1. Lertwassana, W.; Parnklang, T.; Mora, P.; Jubsilp, C.; Rimdusit, S. High Performance Aramid Pulp/carbon Fiber-reinforced Polybenzoxazine Composites as Friction Materials. *Compos. Part B Eng.* **2019**, *177*, 107280. [[CrossRef](#)]
2. Keita, S.; Osamu, T.; Mikiya, T.; Junji, O.; Jun, M.; Toshihiko, N. Research on Prevention of Collapse of Existing Dangerous Masonry Walls by Reinforcement Using Polyurea Resin and Aramid Fiber Tape. In *EASEC16: Proceedings of the 16th East Asian-Pacific Conference on Structural Engineering and Construction, Brisbane, Australia, 23 December 2020*; Springer: Singapore, 2020; Volume 101, pp. 515–528. [[CrossRef](#)]
3. Karthik, K.; Rajamani, D.; Raja, T.; Subramani, K. Experimental Investigation on the Mechanical Properties of Carbon/Kevlar Fibre Reinforced Epoxy LY556 Composites. *Mater. Today Proc.* **2021**, *52*, 668–674. [[CrossRef](#)]
4. He, A.; Xing, T.; Liang, Z.; Luo, Y.; Zhang, Y.; Wang, M.; Huang, Z.; Bai, J.; Wu, L.; Shi, Z.; et al. Advanced Aramid Fibrous Materials: Fundamentals, Advances, and Beyond. *Adv. Fiber. Mater.* **2024**, *6*, 3–35. [[CrossRef](#)]
5. Callomamani, L.A.P.; Bala, N.; Hashemian, L. Comparative Analysis of the Impact of Synthetic Fibers on Cracking Resistance of Asphalt Mixes. *Int. J. Pavement Res. Technol.* **2023**, *16*, 992–1008. [[CrossRef](#)]
6. Hong, C.; Li, H.; Yang, D.; Li, H.; Zhang, H.; Lorenzo, R. Compressive Performance of AFRP Reinforced Laminated Bamboo Stub Columns. *Archiv. Civ. Mech. Eng.* **2022**, *22*, 31. [[CrossRef](#)]
7. Rolland, A.; Chataigner, S.; Benzarti, K.; Quiertant, M.; Argoul, P.; Paul, J.M. Experimental Investigation and Modeling of the Bond between Aramid Fiber-reinforced Polymer Bars and Concrete. *Adv. Civ. Eng. Mater.* **2016**, *5*, 115–128. [[CrossRef](#)]
8. Rubino, F.; Nisticò, A.; Tucci, F.; Carbone, P. Marine Application of Fiber Reinforced Composites: A Review. *J. Mar. Sci. Eng.* **2020**, *8*, 26. [[CrossRef](#)]
9. Qiang, X.; Chen, L.; Jiang, X. Experimental and Theoretical Study on Flexural Behavior of Steel-concrete Composite Beams Strengthened by CFRP Plates with Unbonded Retrofit Systems. *Compos. Struct.* **2023**, *309*, 116763. [[CrossRef](#)]
10. Qiang, X.; Shu, Y.; Jiang, X.; Xiao, Y.; Jin, P. Mechanical Behavior of Carbon Fiber-reinforced Polymer/steel Bonded Joints after Large-space Fires and Thermal Conductivity of Non-intumescent Coatings. *J. Build. Eng.* **2024**, *86*, 108803. [[CrossRef](#)]
11. Chen, L.; Qiang, X.; Sun, P.; Zhang, S.; Jiang, X. Experimental and Theoretical Study on Flexural Behavior of Prestressed Concrete Beams Strengthened by CFRP Tendons with External Unbonded Retrofit System. *J. Build. Eng.* **2024**, *89*, 109301. [[CrossRef](#)]
12. Honickman, H.; Fam, A. Investigating a Structural form System for Concrete Girders Using Commercially Available GFRP Sheet-pile Sections. *J. Compos. Constr.* **2009**, *13*, 455–465. [[CrossRef](#)]
13. Mathieson, H.; Fam, A. High Cycle Fatigue under Reversed Bending of Sandwich Panels with GFRP Skins and Polyurethane Foam Core. *Compos. Struct.* **2014**, *113*, 31–39. [[CrossRef](#)]
14. Sanya, O.T.; Shi, J. Ultra-high-performance Fiber Reinforced Concrete Review: Constituents, Properties, and Applications. *Innov. Infrastruct. Solut.* **2023**, *8*, 188. [[CrossRef](#)]

15. Palola, S.; Vuorinen, J.; Noordermeer, J.W.M.; Sarlin, E. Development in Additive Methods in Aramid Fiber Surface Modification to Increase Fiber-Matrix Adhesion: A Review. *Coatings* **2020**, *10*, 556. [[CrossRef](#)]
16. Kumar, S.; Malek, A.; Babu, R.; Mathur, S. Ballistic Efficiency of Multilayered Armor System Reinforced with Jute-Kevlar Epoxy Composite against High-Energy Steel Core Projectile. *J. Mater. Eng. Perform.* **2021**, *30*, 8447–8464. [[CrossRef](#)]
17. Zhang, B.; Jia, L.; Tian, M.; Ning, N.; Zhang, L.; Wang, W. Surface and Interface Modification of Aramid Fiber and Its Reinforcement for Polymer Composites: A Review. *Eur. Polym. J.* **2021**, *147*, 110352. [[CrossRef](#)]
18. Yang, M.; Zhang, Z.; Yuan, J.; Wu, L.; Li, P.; Zhao, X.; Men, X. Enhanced Mechanical and Tribological Properties of Kevlar/PTFE-phenolic Composites by Improving Interfacial Properties by Aramid Nanofibers. *Polym. Compos.* **2020**, *41*, 4192–4201. [[CrossRef](#)]
19. Zhang, S.; Shi, Z.; Cui, P.; Duan, N.; Li, X. Surface Modification of Aramid Fibers with  $\text{CaCl}_2$  Treatment and Secondary Functionalization of Silane Coupling Agents. *J. Appl. Polym. Sci.* **2020**, *137*, 49159. [[CrossRef](#)]
20. Kandekar, S.B.; Talikoti, R.S. Torsional Behaviour of Reinforced Concrete Beams Retrofitted with Aramid Fiber. *Adv. Concr. Constr.* **2020**, *9*, 1–7. [[CrossRef](#)]
21. Li, Y.-F.; Wang, H.-F.; Syu, J.-Y.; Ramanathan, G.K.; Tsai, Y.-K.; Lok, M.H. Mechanical Properties of Aramid Fiber-reinforced Composites and Performance on Repairing Concrete Beams Damaged by Corrosion. *Songklanakarin J. Sci. Technol.* **2020**, *42*, 637–644.
22. Wiśniewski, D.; Ślōwik, M.; Kempa, J.; Lewandowska, A.; Malinowska, J. Assessment of Impact of Aramid Fibre Addition on the Mechanical Properties of Selected Asphalt Mixtures. *Materials* **2020**, *13*, 3302. [[CrossRef](#)]
23. Bohara, R.P.; Tanapornraweekit, G.; Tangtermsirikul, S. An Experimental Study on Mechanical Properties and Cracking Behaviors of AFRC Used as Functional Material in Hybrid Beams. *Int. J. Civ. Eng.* **2019**, *17*, 1433–1444. [[CrossRef](#)]
24. Zakaib, S.; Fam, A. Flexural Performance and Moment Connection of Concrete-filled GFRP Tube-encased Steel I-sections. *J. Compos. Constr.* **2012**, *16*, 604–613. [[CrossRef](#)]
25. Betts, D.; Sadeghian, P.; Fam, A. Experimental Behavior and Design-oriented Analysis of Sandwich Beams with Bio-based Composite Facings and Foam Cores. *J. Compos. Constr.* **2018**, *22*, 04018020. [[CrossRef](#)]
26. Chen, J.; Zhao, L.; Zhou, K. Improvement in the Mechanical Performance of Multi Jet Fusion-printed Aramid fiber/Polyamide 12 Composites by Fiber Surface Modification. *Addit. Manuf.* **2022**, *51*, 102576. [[CrossRef](#)]
27. Lin, G.; Wang, H.; Yu, B.; Qu, G.; Chen, S.; Kuang, T.; Yu, K.; Liang, Z. Combined Treatments of Fiber Surface Etching/silane Coupling for Enhanced Mechanical Strength of Aramid Fiber-reinforced Rubber Blends. *Mater. Chem. Phys.* **2020**, *255*, 123486. [[CrossRef](#)]
28. Li, Y.; Xie, G.; Li, R.; Wu, Y.; Chen, C.; Luo, Z. Supercritical carbon dioxide assisted impregnation and graft of polyamide acid into aramid fiber for formation of polar interface. *J. Mater. Res. Technol.* **2022**, *21*, 1–11. [[CrossRef](#)]
29. Wang, L.; Zhang, B.; Li, X.; Wang, W.; Tian, M.; Fan, Z.; Zhang, L. Enhanced Adhesion Property of Aramid Fibers by Polyphenol-metal Iron Complexation and Ailane Grafting. *J. Adhes.* **2021**, *97*, 346–360. [[CrossRef](#)]
30. Zuo, L.S.; Li, K.; Ren, D.X.; Xu, M.Z.; Tong, L.F.; Liu, X.B. Surface Modification of Aramid Fiber by Crystalline Polyarylene Ether Nitrile Sizing for Improving Interfacial Adhesion with Polyarylene Ether Nitrile. *Compos. Part B* **2021**, *217*, 107608. [[CrossRef](#)]
31. Han, Y.T.; Tada, K.; Osawa, K.; Uchida, H.; Tamura, K. Surface Modification of Aramid Fiber with Acrylic Acid Assisted by Supercritical Carbon Dioxide. *J. Supercrit. Fluids.* **2023**, *192*, 105787. [[CrossRef](#)]
32. Miao, L.; Wang, X.; Li, S.; Tu, Y.Y.; Hu, J.W.; Huang, Z.Z.; Lin, S.D.; Gui, X.F. An Ultra-Stretchable Polyvinyl Alcohol Hydrogel Based on Tannic Acid Modified Aramid Nanofibers for Use as a Strain Sensor. *Polymers* **2022**, *14*, 3532. [[CrossRef](#)] [[PubMed](#)]
33. Zahra, M.; Zulfiqar, S.; Skene, W.G.; Sarwar, M.I. Crosslinking of Polyamides Using Dianhydrides, Diacid Chloride and Dialdehyde: A Promising Approach for Water Treatment. *Polym. Int.* **2020**, *69*, 50–60. [[CrossRef](#)]
34. Xu, T.; Qi, Z.H.; Yin, Q.; Jiao, Y.M.; An, L.Z.; Tan, Y.F. Effects of Air Plasma Modification on Aramid Fiber Surface and Its Composite Interface and Mechanical Properties. *Polymers* **2022**, *14*, 4892. [[CrossRef](#)] [[PubMed](#)]
35. Sohbatzadeh, F.; Shakerinasab, E.; Mirzanejhad, S. Surface Modification of Aramid Yarn by Atmospheric Pressure Plasma: Reinforcement and Floating Properties. *Polym. Test.* **2023**, *117*, 107836. [[CrossRef](#)]
36. Chen, W.T.; Qi, W.; Du, J.F.; Zhao, L. Radiation Effects on Kevlar Fibers through High Energy Electron beam. *Polym. Eng. Sci.* **2023**, *63*, 3083–3090. [[CrossRef](#)]
37. Jia, C.; Zhang, R.; Yuan, C.; Ma, Z.; Du, Y.; Liu, L.; Huang, Y. Surface Modification of Aramid Fibers by Amino Functionalized Silane Grafting to Improve Interfacial Property of Aramid Fibers Reinforced Composite. *Polym. Compos.* **2020**, *41*, 2046–2053. [[CrossRef](#)]
38. Safamanesh, A.; Mousavi, S.M.; Khosravi, H.; Tohidlou, E. On the low-velocity and high, velocity impact behaviors of aramid fiber/epoxy composites containing modified-graphene oxide. *Polym. Compos.* **2020**, *42*, 608–617. [[CrossRef](#)]
39. Dharmavarapu, P.; Sreekara Reddy, M.B.S. Mechanical, Low Velocity Impact, Fatigue and Tribology Behaviour of Silane Grafted Aramid Fibre and Nano-silica Toughened Epoxy Composite. *Silicon* **2020**, *13*, 1741–1750. [[CrossRef](#)]
40. Chen, Z.; Luo, J.; Huang, Z.; Cai, C.; Tusiime, R.; Li, Z.; Wang, H.; Cheng, C.; Liu, Y.; Sun, Z.; et al. Synergistic Toughen Epoxy Resin by Incorporation of Polyetherimide and Amino Groups Grafted MWCNTs. *Compos. Commun.* **2020**, *21*, 100377. [[CrossRef](#)]
41. Esmaeili, A.; Ma, D.; Manes, A.; Oggioni, T.; Jiménez-Suárez, A.; Ureña, A.; Hamouda, A.; Sbarufatti, C. An Experimental and Numerical Investigation of Highly Strong and Tough Epoxy Based Nanocomposite by Addition of MWCNTs: Tensile and Mode I Fracture Tests. *Compos. Struct.* **2020**, *252*, 112692. [[CrossRef](#)]

42. Sun, H.; Kong, H.; Ding, H.; Xu, Q.; Zeng, J.; Jiang, F.; Yu, M.; Zhang, Y. Improving UV Resistance of Aramid Fibers by Simultaneously Synthesizing TiO<sub>2</sub> on Their Surfaces and in the Interfaces Between Fibrils/Microfibrils Using Supercritical Carbon Dioxide. *Polymers* **2020**, *12*, 147. [[CrossRef](#)] [[PubMed](#)]
43. Zhu, M.H.; Liu, L.; Wang, Z.Z. Mesoporous Silica via Self-assembly of Nano Zinc Amino-tris-(methyleneephosphonate) Exhibiting Reduced Fire Hazards and Improved Impact Toughness in Epoxy Resin. *J. Hazard. Mater.* **2020**, *392*, 122343. [[CrossRef](#)] [[PubMed](#)]
44. Rohit, L.V. A review of ionic liquids: Applications Towards Catalytic Organic Transformations. *J. Mol. Liq.* **2017**, *227*, 44. [[CrossRef](#)]
45. Morales-Rivera, C.A.; Cormack, G.; Burrington, J.; Proust, N.; Mpourmpakis, G. Understanding and Optimizing the Behavior of Al-and Ru-Based Catalysts for the Synthesis of Polyisobutylene Succinic Anhydrides. *Ind. Eng. Chem. Res.* **2022**, *61*, 14462–14471. [[CrossRef](#)]
46. Wang, Y.; Wang, Z.; Yan, Y.; Zhao, X.; Wang, Y. Acylation Reaction of Benzene with Phthalic Anhydride Catalyzed by Amide-AlCl<sub>3</sub> Ionic Liquid Analogs. *Acta Pet. Sin. (Pet. Process. Sect.)* **2022**, *38*, 292. [[CrossRef](#)]
47. Huang, S.; Fu, Q.; Yan, L.; Kasal, B. Characterization of Interfacial Properties between Fibre and Polymer Matrix in Composite Materials—A Critical Review. *J. Mater. Res. Technol.* **2021**, *13*, 1441–1484. [[CrossRef](#)]
48. Koyanagi, J.; Ogihara, S.; Nakatani, H.; Okabe, T.; Yoneyama, S. Mechanical Properties of Fiber/Matrix Interface in Polymer Matrix Composites. *Adv. Compos. Mater.* **2014**, *23*, 551–570. [[CrossRef](#)]

**Disclaimer/Publisher's Note:** The statements, opinions and data contained in all publications are solely those of the individual author(s) and contributor(s) and not of MDPI and/or the editor(s). MDPI and/or the editor(s) disclaim responsibility for any injury to people or property resulting from any ideas, methods, instructions or products referred to in the content.